Enhanced Sampling using Replica Exchange with Non-Equilibrium Switches: A Case Study on Simple Models

Shaunak Badani[1] and Marimuthu Krishnan[1]
Center for Computational Natural Sciences and Bioinformatics (CCNSB),
International Institute of Information Technology, Gachibowli, Hyderabad 500032
India

(*Electronic mail: m.krishnan@iiit.ac.in, shaunak.badani@research.iiit.ac.in)

(Dated: 8 April 2023)

The configurational sampling is central to characterize the equilibrium properties of complex molecular systems, but it remains a significant computational challenge. The conventional molecular dynamics simulations of limited duration often result in inadequate sampling and thus inaccurate equilibrium estimates. Replica exchange with non-equilibrium switches (RENS) is a collective variable-free computational technique to achieve extensive sampling from a sequence of equilibrium and non-equilibrium MD simulations without modifying the underlying potential energy surface of the system. Unlike the conventional replica exchange molecular dynamics (REMD) simulation, which demands a significant number of replicas for better accuracy, RENS employs non-equilibrium heating (forward) and cooling (reverse) work simulations prior to configurational swaps to improve the acceptance probability for replica exchange. Here, we have implemented the RENS algorithm on four model systems and examined its performance against the conventional MD and REMD simulations. The desired equilibrium distributions were generated by RENS for all the model systems, whereas REMD and MD simulations could not do so due to inadequate sampling on the same timescales. The calculated work distributions from RENS obeyed the expected non-equilibrium fluctuation theorem. The results indicate that the switching time of the non-equilibrium simulations can be systematically altered to optimize the acceptance probability and the reduced work of switching. The modular implementation of RENS algorithm not only enables us to readily extend it to multiple replicas, but also paves the way for extension to larger molecular systems in the future.

I. INTRODUCTION

Molecular dynamics (MD) simulation has proven to be a useful computational tool to characterize the equilibrium properties of molecular systems in terms of the underlying governing rules at the atomic level. In MD simulations, the coordinates ($\mathbf{q}$) and momenta ($\mathbf{p}$) of the atoms of an N-particle system are propagated through time by iteratively solving the Hamilton's equations of motion of the system. Since the phase space probability density, $\mathscr{P}(\mathbf{q}, \mathbf{p})$, is proportional to $e^{-\frac{U(\mathbf{q})}{k_B T}}$ (here k_B is the Boltzmann constant, $U(\mathbf{q})$ is the potential energy function, and T is the temperature), only the low energy configurations are sampled well within the limited timescales of MD simulations. Inadequate sampling of the phase space results in poor estimates of MD-derived statistical properties of the system. This sampling problem is more prevalent in large-scale complex systems with highly corrugated potential energy surfaces[1,2]. Thus, long MD simulations would be needed to investigate slow molecular events, but the timescales of such events are typically much higher than what can be realized using state-of-the-art supercomputers[3,4].

A number of computational methods including coarse-grained models[5–8], umbrella sampling[9–11], adaptive biasing force simulations[12–14], metadynamics[15–17], and steered MD[18–20] have been introduced to overcome the sampling problem. However, most of these methods rely on a limited set of collective variables (CVs) to achieve uniform sampling along these specified degrees of freedom. Since most of these methods require *a priori* knowledge of the relevant order parameters or CVs of the system, it is non-trivial to apply them to complex systems with unknown CVs. Moreover, the trajectories obtained from these biased simulations sample some unphysical configurations, which result in a perturbed configurational probability distribution of the system. Consequently, these biased trajectories cannot be readily used to calculate dynamic properties and to investigate dynamical processes involving transitions between different states of the system.

Replica exchange molecular dynamics (REMD)[21], on the other hand, is a non order parameter based sampling method, where multiple replicas of the system are simulated at increasing temperatures to sample microstates from the corresponding equilibrium probability distributions. In REMD, swapping of configurations sampled at different temperatures is a key step to achieve desired equilibrium distribution of the system at a particular temperature. This makes the acceptance probability a critical measure, since it dictates whether a swap between replicas is accepted or rejected. The use of conventional REMD methods requires temperatures to be considered in a manner such that the potential energy distributions of adjacent replicas have a significant overlap, so that swapping between two replicas occurs frequently[22–24]. This requirement imposes a constraint on REMD that, for a system with N_f degrees of freedom, the number of replicas required is proportional to $\sqrt{N_f}$[25]. A number of methods have been proposed as an improvement over standard REMD, such as replica exchange with solute tempering[26], Replica Exchange Umbrella Sampling (REUS)[27] reservoir REMD[28] and replica exchange with dynamical scaling[29].

In the present work, we have explored the replica exchange with non-equilibrium switches (RENS) algorithm, which employs non-equilibrium work simulations to improve the acceptance probability for replica exchange and to achieve extensive phase space sampling. The RENS algorithm used here

is the same as the one originally proposed by Jarzynski and coworkers[30]. A RENS software package is developed from scratch and used to investigate the application of RENS to four different model systems and the results are compared with those obtained from conventional MD and REMD simulations. The molecular characteristics and particle-particle interactions commonly found in several force field potentials are taken into account in some of these models. In addition, the details of the propagator and the Trotter factorization-based integration of equations of motion for the equilibrium MD and the non-equilibrium work simulations are also presented here clearly. Furthermore, the trajectories generated from these RENS simulations are used to validate the Crook's fluctuation theorem for all of the model systems.

II. METHODS

A. RENS algorithm

The RENS algorithm was implemented and applied to four model systems using the protocol as described in Ref. 30. For each system, two replicas were considered at temperatures T_A and T_B ($T_A < T_B$). Initially, NVT simulations of the replicas were performed at their respective temperatures to sample their corresponding canonical distributions. In a typical REMD simulation, configurations are swapped between replicas at regular intervals with an acceptance criterion satisfying the detailed balance condition. However, in RENS, an attempt is made at every step to switch these NVT runs to non-equilibrium work simulations. This attempt is a probabilistic event that is modelled by the Poisson process with an attempt rate $r = 0.166$[30]. That is, an attempt is made to start a work simulation at every step by generating a random number between 0 and 1, and multiplying it with the time step Δt. If this product is less than r ($r = 0.166$ in this case), a non-equilibrium work simulation begins which lasts for τ time. The main purpose of this work simulation is to increase the acceptance probability for configuration swaps between the replicas to be attempted after the work simulation.

B. Work Simulation

In this section, we outline the protocol and the propagation equations used in the work simulation. Each work simulation runs for a total time of τ, during which the system is propagated in time using the following the Hamilton's equations of motion, in conjunction with the Andersen thermostat[30,31]:

$$\dot{\boldsymbol{q}} = \frac{\partial H}{\partial \boldsymbol{p}} \tag{1}$$

$$\dot{\boldsymbol{p}} = -\frac{\partial H}{\partial \boldsymbol{q}} + \dot{\lambda} s_\lambda \boldsymbol{p} \tag{2}$$

Here, $H(\boldsymbol{q},\boldsymbol{p}) = U(\boldsymbol{q}) + K(\boldsymbol{p})$ is the Hamiltonian, $U(\boldsymbol{q})$ is the potential energy, $K(\boldsymbol{p})$ is the kinetic energy, $\boldsymbol{q}$ and $\boldsymbol{p}$ are the generalized coordinates and momenta of the system, respectively. $\lambda(t) = \frac{t}{\tau}$ is a time-dependent parameter that switches from 0 (corresponding to t=0) to 1 (corresponding to t=τ) in time τ and its time derivative is denoted by $\dot{\lambda}$. The time t here is local to the work simulation such that $t = 0$ and $t = \tau$ denote the start and end of a work simulation. That is, t is set to 0 at the start of every work simulation. Each RENS run consists of a series of alternating equilibrium MD simulation (for a duration of τ_{eq}) and the non-equilibrium work simulation (for a duration of τ) runs. The fraction of time devoted to work simulation is denoted by f_{sw}, which is defined as follows:

$$f_{sw} = \frac{\tau}{\tau_{eq} + \tau} \tag{3}$$

As τ increases, the fraction of time devoted to work simulation also increases. The λ-dependent temperature $T_\lambda = T_A + \lambda(T_B - T_A)$ of the system at a given λ is linearly interpolated between T_A and T_B. s_λ is defined as follows :

$$s_\lambda = \frac{1}{2T_\lambda}\frac{dT_\lambda}{d\lambda} = \frac{1}{2T_\lambda}(T_B - T_A) \tag{4}$$

s_λ dictates the magnitude of the increase or decrease of the momenta during the work simulation. s_λ is positive for a work simulation in which the low-temperature replica is gradually heated from the low temperature (T_A) to the high temperature (T_B). In what follows, this kind of work simulation is referred to as the heating work (or forward) simulation. Given that the time derivative of λ is always positive, a positive s_λ would imply scaling up of momenta of the particles based on the difference between T_A and T_B during the heating work simulation. Similarly, the momenta are scaled down during the cooling work (or reverse) simulations, in which the high-temperature replica is gradually cooled from the high temperature to the low temperature. s_λ is negative for the cooling work simulations.

To derive the integrator for the above equations of motion, let $\Gamma(0) = \Gamma(\mathbf{p}(0), \mathbf{q}(0))$ and $\Gamma(\Delta t) = \Gamma(\mathbf{p}(\Delta t), \mathbf{q}(\Delta t))$ denote the phase space vectors corresponding to the microstates of a system at times 0 and Δt, respectively. The time evolution of the system is governed by the following equation:

$$\Gamma(\Delta t) = e^{iL\Delta t}\Gamma(0) \tag{5}$$

where $iL = \dot{\mathbf{q}}.\frac{\partial}{\partial \mathbf{q}} + \dot{\mathbf{p}}.\frac{\partial}{\partial \mathbf{p}}$ is the Liouville operator[32]. If $iL_1 = \dot{\mathbf{q}}.\frac{\partial}{\partial \mathbf{q}}$ and $iL_2 = \dot{\mathbf{p}}.\frac{\partial}{\partial \mathbf{p}}$, then using the Trotter's factorization[33], we obtain the following evolution equation :

$$\Gamma(\Delta t) = e^{iL_2\Delta t/2} e^{iL_1\Delta t} e^{iL_2\Delta t/2}\Gamma(0) \tag{6}$$

which leads to the following update equations for the positions

and momenta of all the particles in the system (see Appendix):

$$\mathbf{p}(\frac{\Delta t}{2}) = \mathbf{p}(0)e^{\frac{z\Delta t}{2}} + \mathbf{F}(\mathbf{q}(0))\frac{(e^{\frac{z\Delta t}{2}}-1)}{z} \quad (7)$$

$$\mathbf{q}(\Delta t) = \mathbf{q}(0) + \frac{\mathbf{p}(\frac{\Delta t}{2})}{m}\Delta t \quad (8)$$

$$\mathbf{p}(\Delta t) = \mathbf{p}(\frac{\Delta t}{2})e^{\frac{z\Delta t}{2}} + \mathbf{F}(\mathbf{q}(\Delta t))\frac{(e^{\frac{z\Delta t}{2}}-1)}{z} \quad (9)$$

where $z = \dot{\lambda} s_\lambda$.

The above Trotter factorization-based integrator differs from the standard scaling method, $\mathbf{p}(\Delta t) = \mathbf{p}(0)(T_{\lambda(\Delta t)}/T_{\lambda(0)})^{1/2}$, commonly used in REMD and RENS simulations. However, the correspondence between these two methods can be demonstrated as follows. In the limit $\Delta t \to 0$, $e^{\frac{z\Delta t}{2}} \approx 1 + \frac{z\Delta t}{2} \approx \sqrt{1+z\Delta t}$, and thus equation 7 can be written as:

$$\mathbf{p}(\frac{\Delta t}{2}) = \mathbf{p}(0)\sqrt{\frac{T_{\lambda(\frac{\Delta t}{2})}}{T_{\lambda(0)}}} + \mathbf{F}(0)\frac{\Delta t}{2} \quad (10)$$

where $T_{\lambda(t)} = T_A + (T_B - T_A)\frac{t}{\tau}$ and $z = (T_B - T_A)\frac{1}{2\tau T_\lambda}$. Correspondingly, in the limit $\Delta t \to 0$, the resultant momentum update equation can be written as follows:

$$\mathbf{p}(\Delta t) = \mathbf{p}(0)\sqrt{\frac{T_{\lambda(\Delta t)}}{T_{\lambda(0)}}} + \left(\sqrt{\frac{T_{\lambda(\Delta t)}}{T_{\lambda(\frac{\Delta t}{2})}}}\mathbf{F}(0) + \mathbf{F}(\Delta t)\right)\frac{\Delta t}{2} \quad (11)$$

This update equation reduces to the standard scaling form when $U(\mathbf{q}) = 0$. Thus, for a free-particle system, the scaling protocol is *exactly* equivalent to the update equations derived here.

The work simulation consists of the above update equations in conjunction with the Andersen thermostat. During the work simulation at a given λ, the atomic velocities are sampled at a regular time interval (500 steps) from the Maxwell-Boltzmann velocity distribution corresponding to the λ-dependent temperature T_λ. The algorithmic details of RENS (*RENS* (**Algorithm 1**), *WorkSimulation* (**Algorithm 2**), *WorkIntegrator* (**Algorithm 3**), and *AndersenUpdate* (**Algorithm 4**)) presented in the Appendix along with Figure 2 and Figure 1 explain the detailed protocol used for RENS and non-equilibrium work simulations. All the variables and parameters involved in these algorithms are defined in Table II.

The *Thermostat* function is a propagator for the equilibrium NVT runs. We used both the Nose-Hoover thermostat[34,35] and the Langevin thermostat[36] to control the temperature of a given system. The implementation of RENS reported here assumes only two replicas for the RENS simulation. The *recv* and *Exchange* functions enable replicas to exchange information about their temperatures and swapping phase space vectors, respectively. The acceptance probability is calculated for one replica, and its value is communicated to the other replica.

The reduced work is calculated for each work simulation and the sum of the reduced work for the heating and cooling work simulations is then used to calculate the acceptance probability, which is defined as

$$P_{acc} = min(1, e^{-w_H - w_C}) \quad (12)$$

where w_H and w_C denote the reduced work for the heating and cooling work simulations, respectively. If the replica swap is successful, then the end states of the work simulations are swapped. However, if the swap fails, then the current work simulations are ignored, the phase space vectors of replicas are reverted back to their values at the beginning of the work simulations, and the equilibrium MD runs are continued from there on (Figure 1).

III. SIMULATION DETAILS

The RENS runs were performed on four model systems, which are labelled as Model-I, Model-II, Model-III, and Model-IV, the details of which are provided in the following sections. The molecular characteristics and particle-particle interactions commonly found in several force field potentials are taken into account in some of these model systems. Except Model-I, all the remaining models are novel and the RENS algorithm has never been applied to them before. Model-I was taken from the work of Jarzynski and coworkers[30] to validate our implementation by ensuring that the results are consistent with those of the original paper.

In the current implementation of RENS, we have used the following reduced units for Models I-III: the Boltzmann constant k_B=1, the particles considered are of unit mass and their velocities are such that $\sum_{i=1}^{N} |\mathbf{v}_i|^2 = N_f T$, where N_f is the number of degrees of freedom of the system, and T is the dimensionless temperature, and all the energies are expressed in the units of $k_B T$. For model IV, molecular units ($k_B = 8.311\,74 \times 10^{-3}\,\mathrm{kJ\,mol^{-1}\,K^{-1}}$, Å for the atomic positions, and $\mathrm{Å\,ps^{-1}}$ for the atomic velocities) are used.

A. Model-I: One-dimensional System

The first model is a one-dimensional system, in which N non-interacting particles are moving on a one-dimensional potential energy surface, $U(x)$, defined as follows[37]:

$$U(x) = \begin{cases} 4\pi^2\,(x+1.25)^2 & x \le -1.25 \\ 2\,(1+\sin(2\pi x)) & -1.25 < x \le -0.25 \\ 3\,(1+\sin(2\pi x)) & -0.25 < x \le 0.75 \\ 4\,(1+\sin(2\pi x)) & 0.75 < x \le 1.75 \\ 8\pi^2\,(x-1.75)^2 & x > 1.75 \end{cases} \quad (13)$$

For a position vector $\boldsymbol{x} = [x_1, x_2, ..., x_N]$, where x_i denotes the position of the i^{th} particle, we have

$$U(\boldsymbol{x}) = \sum_{i=1}^{N} U(x_i) \quad (14)$$

This potential energy surface consists of four energy wells

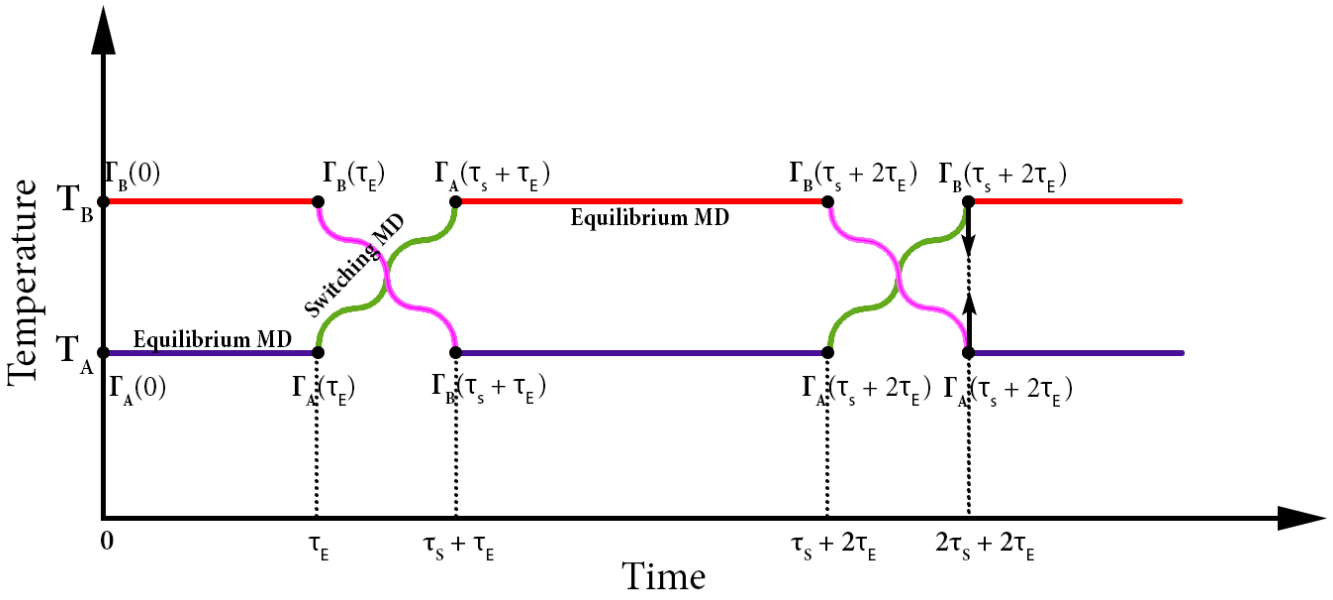

FIG. 1: RENS consists of a series of alternating equilibrium MD (for a duration of τ_E) and the non-equilibrium switching MD (for a duration of τ_S; here $\tau_S = \tau$) runs. Two work simulations are shown here. The first one denotes a successful swap after the completion of switching MD, after which the phase space vectors (Γ_A and Γ_B) at the end of the switching protocol are exchanged, and equilibrium MD follows. The second switching protocol denotes a failed swap. The configuration at the beginning of the switching protocol is used to continue equilibrium sampling for each of the replicas.

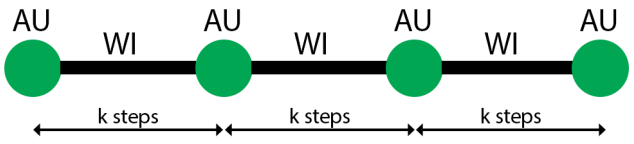

FIG. 2: The protocol followed in a work simulation. At every k steps, the *AndersenUpdate* (AU) subroutine is called, which performs an Andersen update for a randomly selected particle at temperature T_λ. In between every two successive Andersen updates, the system evolves with time in a deterministic manner according to the *WorkIntegrator* (WI) subroutine called in succession.

(Figure 3) and transitions between these wells can be used to validate whether the RENS protocol provides adequate sampling of all the energy wells. We performed equilibrium NVT MD runs at two different temperatures ($T = 0.3$ and $T = 2$) to assess the temperature dependence of the degree of sampling of these wells. The low-temperature MD resulted in particles being confined to the well they are initialized in, while the particles could undergo transitions between the wells at $T = 2.0$. The aim of enhanced sampling methods is to achieve equilibrium sampling at $T = 0.3$. REMD could be used for this purpose, but is limited to exchanging configurations only for significant acceptance probability criterion. With RENS, we aim to improve the acceptance probability, P_{acc}, for replica exchange and thereby sample all the energy wells of this model system at $T = 0.3$.

In addition to the aforementioned equilibrium NVT MD runs, we performed both REMD and RENS on Model-I using two replicas at temperatures $T_A = 0.3$ and $T_B = 2.0$ for a total of 10^9 steps, with $dt = 10^{-3}$, and $N = 10$. For the temperature control, we used both the Nose-Hoover chain (NHC) of 4 thermostats[32] and the Langevin thermostat independently. For NHC, an initialization of $xi = [0,0,0,0]$ and $vxi = [-1.0, 1.0, -1.0, 1.0]$ was adapted from ref. 36. Here xi and vxi denote the initial positions and momenta of the four NHC thermostats. A friction coefficient of $\gamma = 0.05$[36] was used for the Langevin thermostat. While both the NHC and Langevin thermostats were able to reproduce the expected canonical distribution for the two replicas, due to better accuracy we present here only the results obtained using the Langevin thermostat.

B. Model-II: Two-dimensional System

In Model-II, we considered a modified Müller-Brown potential energy surface, $U_{MMB}(x,y)$, which is defined as follows:

$$U_{MB}(x,y) = \sum_{i=1}^{4} A_i e^{a_i(x-\bar{x}_i)^2 + b_i(x-\bar{x}_i)(y-\bar{y}_i) + c_i(y-\bar{y}_i)^2}$$
$$U_{MMB}(x,y) = U_{MB}(x,y) + he^{-\frac{(x+0.25)^2+(y-0.65)^2}{2\sigma^2}} \quad (15)$$

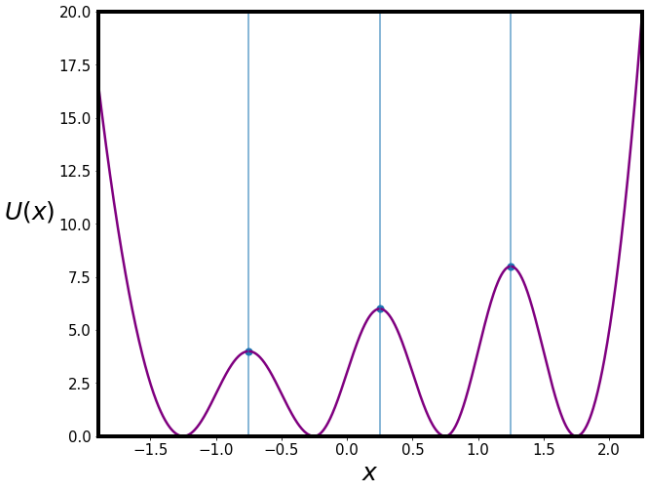

FIG. 3: The one-dimensional potential energy surface $U(x)$ used in Model-I. The vertical lines separate the four energy basins.

where $U_{MB}(x,y)$ is the original Müller-Brown potential energy surface (MBPES), which is commonly used to test algorithms that find reaction pathways and saddle points on complex energy landscapes[38–40]. All the parameters of the above equations are provided in Table I.

$U_{MB}(x,y)$ consists of three minima located at (-0.558, 1.44), (-0.05, 0.467), and (0.6235, 0.0280). The deeper energy basin centered at (-0.558, 1.44) has a higher expected probability density than the other two energy wells. On the other hand, $U_{MMB}(x,y)$, which is generated by adding an extra Gaussian term centered at (-0.25, 0.65) with width $\sigma = 0.8$ and height $h = 200$ to $U_{MB}(x,y)$, consists of two distinct wells centered at (-0.451, 1.591) and (0.777, 0.0035) that are separated by a significant energy barrier.

In order to decide on suitable temperatures for the replicas, we performed unbiased NVT runs on Model-II at different temperatures ($T = 3, 7, 10, 15, 20, 50$). The temperatures of the replicas needed for REMD and RENS should be chosen such that both energy wells of $U_{MMB}(x,y)$ are sampled incompletely at the lower temperature (T_A), while sampling of both wells is adequate at the higher temperature (T_B). Based on examination of the behaviour of the system at different temperatures, 7 and 20 were chosen as T_A and T_B, respectively, for this model.

For this model, REMD and RENS runs were performed for 10^9 steps with $dt = 0.001$ for a system of $N = 10$ non-interacting particles. 14 different τ values ranging from 0 to 100 were considered for RENS runs. A Langevin thermostat was used for equilibrium sampling, with a friction coefficent of $\gamma = 0.05$.

C. Model-III: LEPS-II system

The LEPS-II potential energy surface, which has frequently been used to represent activated processes coupled to a medium, such as a chemical reaction in a solution or in a solid matrix, has been considered as Model-III[41]. This potential describes a system of four interacting particles (labelled as A, B, C, and D). In this model, the distance between A and C is fixed ($r_{AC} = 3.742$), B is harmonically coupled to D via a bond stretching harmonic potential, and B is free to move along a straight line between A and C. Essentially, this model mimics the bond dissociation/association reaction in which B shuttles between A and C.

TABLE I: Parameters used in the Modified Müller-Brown PES

Parameter	Values
$\boldsymbol{A}$	[-200, -100, -170, 15]
$\boldsymbol{a_i}$	[1, 0, -0.5, -1]
$\boldsymbol{b_i}$	[0, 0, 11, 0.6]
$\boldsymbol{c_i}$	[-10, -10, -6.5, 0.7]
$\boldsymbol{x_i}$	[1, 0, -0.5, -1]
$\boldsymbol{y_i}$	[0, 0.5, 1.5, 1]

The mathematical form of LEPS-II potential is as follows :

$$U_{LEPS\_II}(r_{AB},x) = U_{LEPS\_I}(r_{AB}, r_{AC} - r_{AB}) + 2k_c(r_{AB} - (r_{AC}/2 - x/c))^2 \tag{16}$$

where U_{LEPS_I} is defined as follows :

$$U_{LEPS\_I}(r_{AB},r_{BC}) = \frac{Q(r_{AB})}{1+a} + \frac{Q(r_{BC})}{1+b} + \frac{Q(r_{AC})}{1+c} - \left[\frac{J^2(r_{AB})}{(1+a)^2} + \frac{J^2(r_{BC})}{(1+b)^2} + \frac{J^2(r_{AC})}{(1+c)^2} - \frac{J(r_{AB})J(r_{BC})}{(1+a)(1+b)} - \frac{J(r_{BC})J(r_{AC})}{(1+b)(1+c)} - \frac{J(r_{AB})J(r_{AC})}{(1+a)(1+c)}\right]^{\frac{1}{2}} \tag{17}$$

where r_{AB}, r_{BC} are A-B and B-C distances, respectively, x is the B-D distance, the Coulomb interaction between electron clouds is denoted by the $Q(r)$ function, and the quantum mechanical exchange interactions are represented by $J(r)$. The $Q(r)$ and $J(r)$ functions are defined as follows :

$$Q(r) = \frac{d}{2}\left(\frac{3}{2}e^{-\alpha(r-r0)} - e^{-\alpha(r-r0)}\right)$$
$$J(r) = \frac{d}{4}\left(e^{-\alpha(r-r0)} - 6e^{-\alpha(r-r0)}\right) \tag{18}$$

The parameters of the LEPS-II potential have been taken from[41], except for the value of b, which was taken to be 0.03 instead of 0.8, and c, which was taken to be 1.154 for both LEPS and the harmonic part. A comprehensive list of these parameters is as follows : $d_{AB} = d_{BC} = 4.746$, $d_{AC} = 3.445$, $a = 0.05$, $b = 0.03$, $c = 1.154$, $r0$ for all three pairs $= 0.742$, α for all three pairs $= 1.942$, $k_C = 0.2025$, $r_{AC} = 3.742$.

The contour plot of the LEPS-II potential energy surface shown in Figure 5 exhibits two distinct energy wells: the first well is around the minimum at (0.741, 1.303) and the second

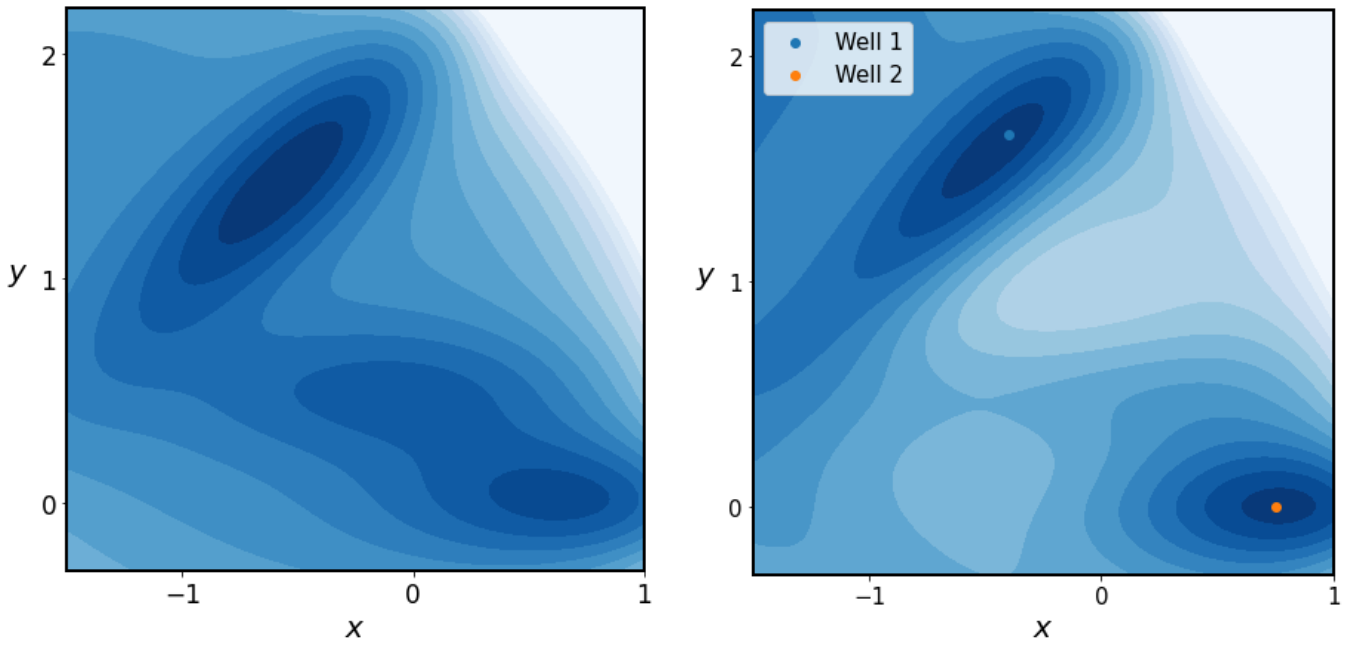

(a) Müller-Brown PES

(b) Modified Müller-Brown PES

FIG. 4: Contour plots for the Müller-Brown PES (left) and for the modified Müller-Brown PES (right).

well is around the minimum at (3.001, -1.303). The first minimum corresponds to the reactant state in which B is bonded to A and C is far from B with $r_{AB} = 0.741$ and $r_{BC} = 3.001$. The second minimum corresponds to the product state in which B is bonded to C and A is far from B with $r_{AB} = 3.001$ and $r_{BC} = 0.741$. The contribution of the harmonic potential arising from the B-D bond is negligible at these minima.

As before, a series of equilibrium MD runs were performed on Model-III at different temperatures to decide on T_A and T_B. At T_A=0.3, the system sampled only the basin in which it was initialized, whereas both the wells were sampled at T_B=1. Thus, 0.3 and 1.0 were chosen as T_A and T_B, respectively, for this model. RENS runs were performed on Model-III for the same 14 values of τ considered for Model-I and Model-II, each for 10^9 steps. An REMD run was also carried out at the same thermodynamic conditions. The Langevin thermostat was used, with a friction coefficient $\gamma = 0.05$.

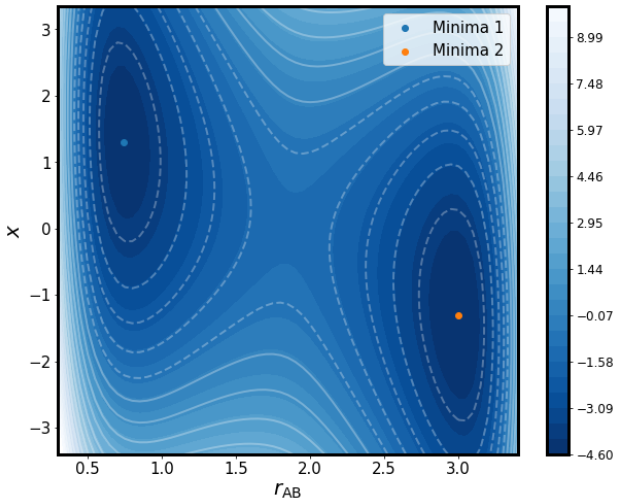

FIG. 5: Contour plot of the LEPS-II potential.

D. Model-IV : Lennard-Jones System

We consider an N-particle system of Lennard-Jones (LJ) particles as Model-IV. This system consists of 108 particles confined in a cubic volume $V = 5258.039\,\text{Å}^3$ and kept at a constant temperature T. The interaction energy between a pair of particles is given by:

$$U = \sum_{i=1}^{N-1} \sum_{j=i+1}^{N} 4\varepsilon((\sigma/r_{ij})^{12} - (\sigma/r_{ij})^{6}) \qquad (19)$$

where r_{ij} denotes the distance between the particles i and j, σ is the diameter of a particle, and ε is the well depth. The values of ε and σ are $0.997\,\text{kJ mol}^{-1}$ and 3.4 Å, respectively[42]. The mass of a particle is 39.95 u. $T_A = 80\,\text{K}$ and $T_B = 105\,\text{K}$ were considered as the two temperatures for RENS simulations. $T_A = 80\,\text{K}$ was chosen to model the phase of argon near its triple point (83.8 K), where the dynamics is highly restricted[43]. On the contrary, $T_B = 105\,\text{K}$ is closer to the liquid-gas coexistence region, where argon exhibits facile dynamics. Three-dimensional periodic boundary conditions were used in all the calculations. The Langevin thermostat

was used with a damping coefficient of $\gamma = 0.05\,\mathrm{ps}^{-1}$. RENS simulations were carried out from an energy minimized configuration of the system with a time step of $dt = 10^{-3}$ps, for 10^8 steps.

IV. RESULTS AND DISCUSSION

A. Mean Work and Acceptance Probability

As indicated before, the primary objective of RENS is to increase the acceptance probability for configuration swaps between replicas with minimal reduced work during the work simulation. The variation of the mean work and the average acceptance probability with the fractional switching time (f_{sw} defined in Eq. 3) for all the models are shown Figure 6. The work reported here is the mean of the reduced work $w = w_H + w_C$, where w_H and w_C denote the work computed from the heating and cooling work simulations, respectively.

The mean reduced work is calculated from multiple work simulations carried out at a given τ. The results presented here are obtained from multiple RENS runs performed at different τ values (10 different τ values for Model-IV and 14 each for the remaining models) When $\tau = 0$, RENS reduces to REMD, in which case the acceptance probability is negligibly small for all the model systems. However, the average acceptance probability increases and the mean work decreases with increasing τ for all the models. The increase in the acceptance probability is gradual up to $\tau \sim 5$ for Model-I, but beyond which it begins to increase abruptly. The calculated acceptance probability at a given f_{sw} for Model-II is less than that for Model-I. This result is attributed to the fact that the acceptance probability also critically depends on the temperature difference between the chosen replicas; the higher the temperature difference, the lower is the acceptance probability. In our calculations, the temperature difference for Model-II is significantly higher than that for Model-I.

To examine the temperature dependence of the mean acceptance probability, we performed another RENS simulation with $T_A = 7$ and $T_B = 12$ for Model-II. The temperature difference between these replicas is significantly less than that for the run with $T_A = 7$ and $T_B = 20$. As expected, the mean acceptance probability calculated from the RENS run with $T_B = 12$ is higher than that for the former run with $T_B = 12$ at all τ values.

The general trend of increasing mean acceptance probability and decreasing mean work with increasing f_{sw} is also observed for the Models III and IV. However, the dependence of the mean work and the acceptance probability on f_{sw} appears to be sensitive to the nature of the underlying potential energy surface.

Although a larger switching time guarantees a higher acceptance probability, every step of the work simulation demands equilibrium sampling from the canonical distribution at the corresponding T_λ. That is, for a RENS simulation performed for time t_{max} with n work simulations at a given τ, n NVT simulations of $\frac{t_{max}-n\tau}{n}$ duration would be required at the respective replica temperatures. The above formula has been calculated, taking into consideration that for every NVT run, there is a corresponding work simulation that follows, including the last NVT run of the simulation. The larger the τ the shorter would be equilibration time for these NVT runs. As equilibrium sampling time decreases, number of points sampled from the canonical ensemble decreases. As a result, the probability distribution obtained from the sampled points deviates further from the expected distribution.

B. Probability Distribution

The probability distribution calculated from RENS trajectories (excluding configurations obtained from work simulations) for a temperature of interest is compared with the expected distribution for Model-I (Figure 7), Model-II (Figure 8) and Model-III (Figure 9). The expected probability distribution is calculated using the following equation

$$\rho(\mathbf{q}) = \frac{e^{-\beta U(\mathbf{q})}}{Z} \tag{20}$$

where $Z = \int_{-\infty}^{\infty} e^{-\beta U(\mathbf{q})} d\mathbf{q}$ is the configurational partition function, $\beta = \frac{1}{k_B T}$, k_B is the Boltzmann constant, T is the temperature, $\mathbf{q}$ is the set of coordinates, and $U(\mathbf{q})$ is the potential energy of the system. For Model-I, $\mathbf{q} = x$, $U(\mathbf{q}) = U(x)$, $d\mathbf{q} = dx$ and those for Model-II and III, are $\mathbf{q} = (x,y)$, $U(\mathbf{q}) = U_{MMB}(x,y)$, $d\mathbf{q} = dxdy$. This probability distribution was obtained for a tagged particle of Model-I from RENS trajectory with $\tau = 2$, and the result is shown in Figure 7(b).

The probability distributions for Model-I show four peaks corresponding to 4 different energy wells. The RENS-derived distribution overlaps reasonably well with the expected distribution than that obtained from REMD. For Model-II, the probability distributions for a tagged particle calculated from REMD and RENS trajectories are compared with the expected probability distribution in Figure 8. It is evident that the RENS algorithm, for the same number of steps, yields a better probability distribution than REMD. Figure 8 also reveals that the REMD run was not able to sample the 2nd well sufficiently enough, due to low acceptance probability across the 2 temperatures. The RENS run was able to sample both energy wells reasonably well within the time scale of the simulation. RENS was able to perform relatively well even for Model-III and Model-IV.

To compare the degree of convergence of sampling, the Kullback-Liebler divergence (KL_{div}) was calculated using the expected and computed probability distributions as follows[44,45]:

$$KL_{div} = \sum_i p_i \log(\frac{p_i}{q_i}) \tag{21}$$

where p denotes the true probability distribution, and q denotes the computed probability distribution for a single particle. KL_{div} would be zero if the expected and calculated probability distributions are equal, which serves as an ideal con-

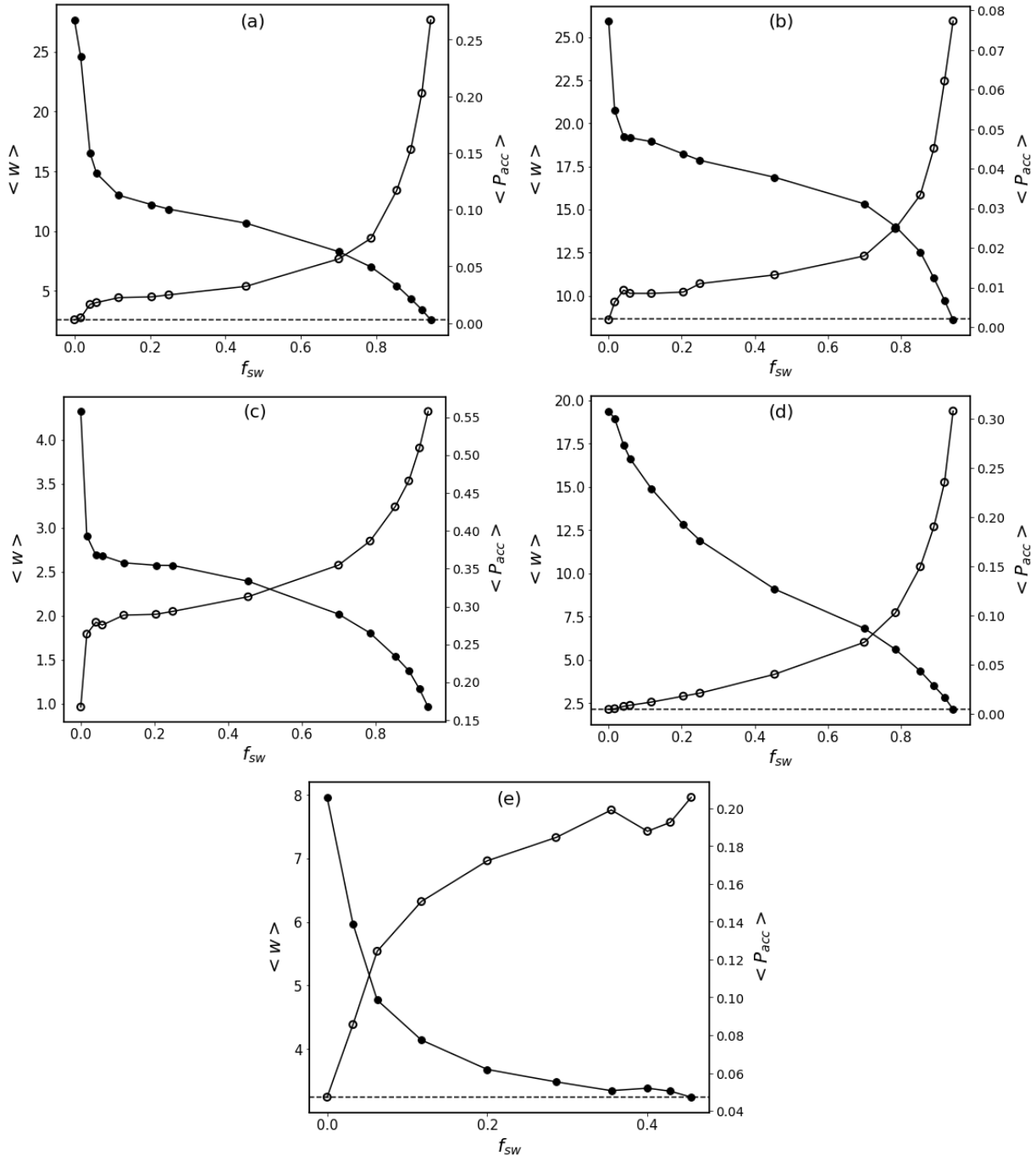

FIG. 6: f_{sw}-dependence of the mean acceptance probability (open circle) and reduced work (filled circle) for (a) Model-I, (b) Model-II (with T_A =7 and T_B =20), (c) Model-II (with T_A =7 and T_B =12), (d) Model-III and (e) Model-IV. The corresponding mean acceptance probabilities (dashed line) obtained from REMD simulation are also shown.

vergence criterion for RENS simulation. The probability distribution is calculated for each particle separately from RENS trajectories and using these single-particle probability distribution functions the KL divergence is computed for each particle. Based on the degree of sampling, the KL divergence would differ across particles. The particles that exhibit reasonable sampling are expected to have lower KL_{div} values, while those with inadequate sampling are likely to have higher KL_{div} values. A mean of KL_{div} was taken across all N particles to obtain $\langle KL_{div} \rangle$ for a simulation. For all practical purposes, a RENS simulation is said to be converged if the mean KL_{div} reaches a lower threshold value.

Figure 1 (a), (b) and (c) in the supplementary information shows KL_{div} of individual particles calculated from REMD

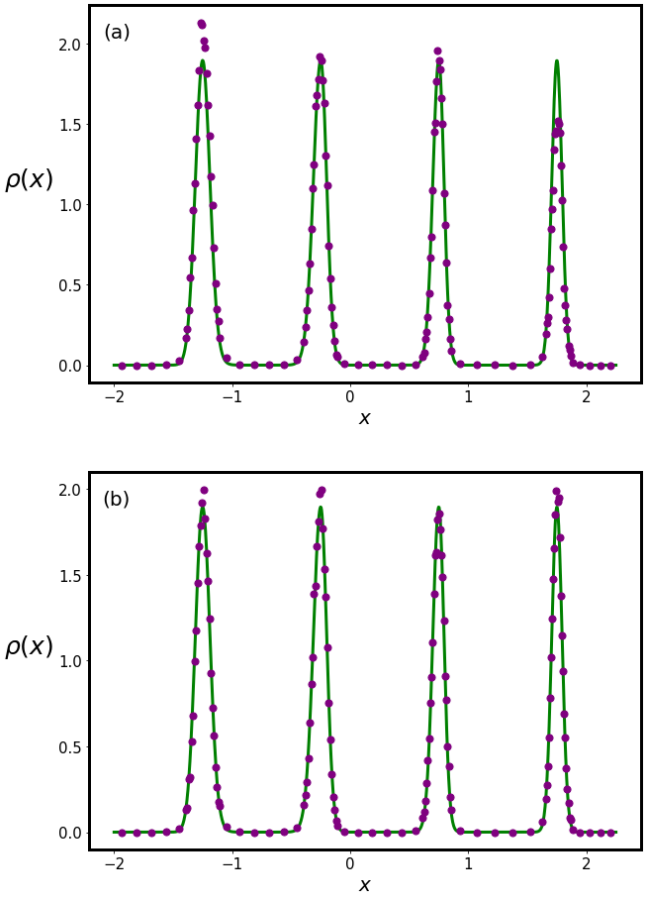

FIG. 7: The expected (solid line) and calculated (filled circles) probability distributions for a tagged particle of Model-I obtained from the (a) REMD and (b) RENS simulations.

(black) and RENS (red) with $\tau = 2$, for Model-I, $\tau = 5$ for Model-II, and $\tau = 2$ for Model - III shown along with their averages (dashed red lines). The KL_{div} obtained from REMD is significantly higher than that calculated from RENS for many particles. This is because for the same length of RENS simulation, a higher value of τ indicates lesser time for NVT sampling, and therefore, lesser number of total samples in the output trajectory.

The increase in $\langle KL_{div} \rangle$ in Figure 10 (b) and (c) is due to more time being devoted to work simulations, and less time towards equilibrium sampling, as the total simulation time is the same for all RENS simulations. Calculation of the probability distributions was not done for the Lennard-Jones system (Model-IV), as it is a $3N$ dimensional function.

C. Non-equilibrium Fluctuation Theorem

Each work simulation performed during RENS is a non-equilibrium process, which transforms the canonical distribution either from T_A to T_B (heating) or from T_B to T_A (cooling).

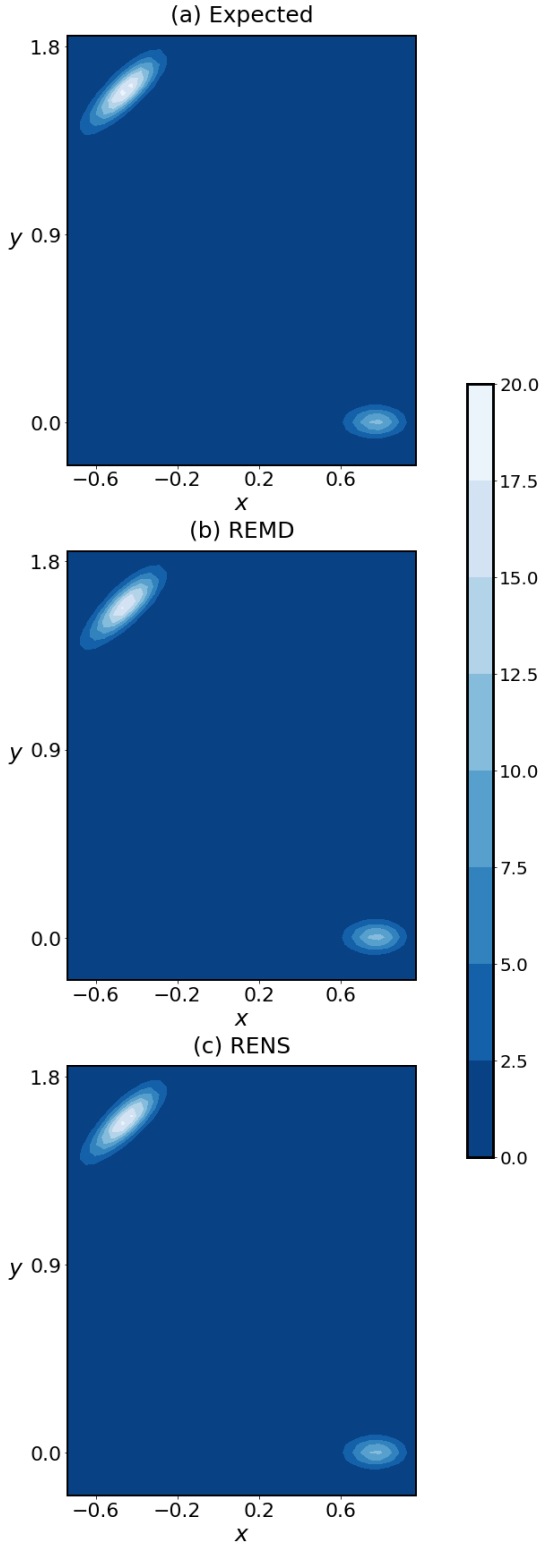

FIG. 8: The (a) expected and calculated (using (b) REMD and (c) RENS) probability distributions for a tagged particle of Model-II.

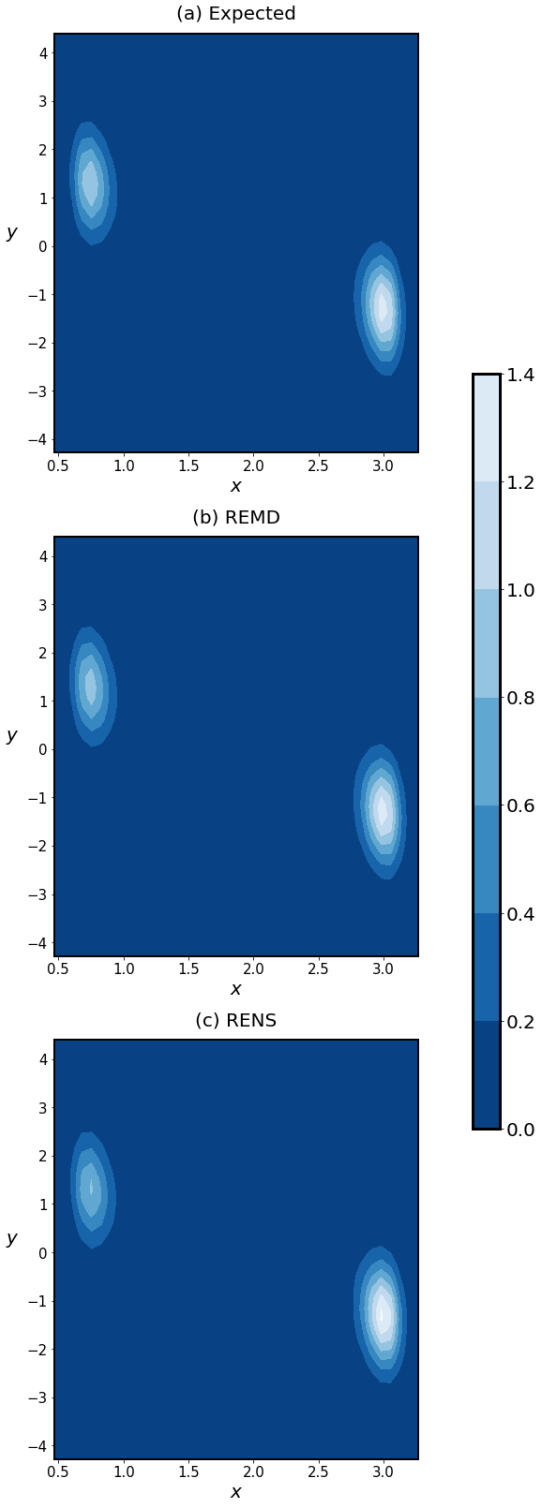

FIG. 9: The (a) expected and calculated (using (b) REMD and (c) RENS) probability distributions for simulations performed using a single particle in the modified LEPS-II potential as described before.

Throughout the course of RENS, multiple work simulations are carried out between the two temperatures, and different reduced work values are obtained. Let $\rho_H(w)$ and $\rho_C(-w)$ denote the computed reduced work distributions for the heating and cooling work simulations, respectively. In order to validate our calculation of the reduced work and its distribution, we examined whether $\rho_H(w)$ and $\rho_C(-w)$ satisfy the Crooks fluctuation theorem (CFT)[46], which is defined as follows:

$$\frac{\rho_H(w)}{\rho_C(-w)} = e^{w-\Delta f} \tag{22}$$

where $\Delta f = f_B - f_A$ denotes the reduced free energy difference between the replicas and the reduced free energy of the replica i is calculated as follows:

$$f_i = -\ln \int_{\mathbf{x}} e^{-h_i(\mathbf{x})} d\mathbf{x} \tag{23}$$

where $h_i(\mathbf{x}) = \frac{H(\mathbf{x})}{k_B T_i}$ is the reduced Hamiltonian of the replica i simulated at temperature T_i, and $\mathbf{x} = [\mathbf{q}, \mathbf{p}]$ with $d\mathbf{x} = d\mathbf{q}d\mathbf{p}$. The reduced work distributions calculated for Model-I, Model-II, Model-III and Model-IV are shown in Figure 11 (a), (b), (d) and (e) respectively. The free energy difference Δf calculated from the partition function (using Eqn. 23) precisely coincides with the point of intersection of $\rho_H(w)$ and $\rho_C(-w)$ for all model systems.

For a more stringent validation of CFT, the overlapping distributions test was carried out for all the model systems using the protocol as described in ref.[47,48]. In this approach, the computed heating and cooling work distributions are used to define the following functions:

$$\begin{aligned} L_H(w) &= \ln \rho_H(w) - \frac{w}{2} \\ L_C(w) &= \ln \rho_C(-w) + \frac{w}{2} \end{aligned} \tag{24}$$

As per CFT, the difference of these two functions ($\Delta L(w) = L_C(w) - L_H(w)$) should be equal to the reduced free energy difference (Δf) as given below:

$$\Delta L(w) = L_C(w) - L_H(w) = \Delta f \tag{25}$$

Thus, the difference function $\Delta L(w)$ is expected to be a constant function of w in the overlap region of the work distributions. The calculated $\Delta L(w)$ as a function of $w_\Delta = \frac{w - w_{min}}{w_{max} - w_{min}}$ for all the model systems are presented in Fig. 12. Here, w_{min} and w_{max} denote the minimum and maximum values of w respectively for each individual system. $\Delta L(w)$ vs w plots are provided for individual systems in the supplementary information (Figure 2). As expected, $\Delta L(w) - \Delta f$ fluctuates about zero in the overlapping region for all the model systems studied.

For the Lennard Jones system, we plotted the work distributions for all 10 RENS runs, performed at different τ values. These plots can be found in the supplementary information (Figure 3). All of the 10 distributions seemed to agree at the value of the intersection point, which was around 170.6. This

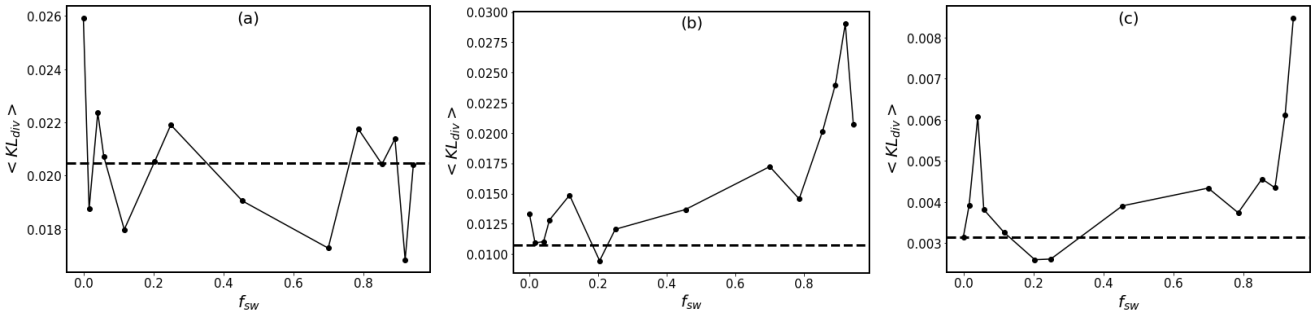

FIG. 10: RENS-derived f_{sw}-dependence of $\langle KL_{div}\rangle$ (solid line) is compared with $\langle KL_{div}\rangle$ obtained from REMD (dashed black line) for (a) Model-I, (b) Model-II, and (c) Model-III.

value is likely to be the reduced free energy difference for the Lennard-Jones system between temperatures $T_A = 80$ and $T_B = 105$.

V. CONCLUSION

The configurational sampling of complex molecular systems remains a significant computational challenge, but it is required to characterize the equilibrium properties of such systems at the microscopic level. The conventional equilibrium MD simulations of limited duration tend to sample the configurational space inadequately. To overcome this sampling problem, various computational methods have been developed and a majority of them essentially modify the underlying potential energy surface using bias potentials to enhance the sampling. Moreover, they seek to achieve sufficient sampling along a predefined set of collective variables, while the extent of sampling of other degrees of freedom also plays a non-negligible role in improving the accuracy of these methods. On the contrary, by exchanging equilibrium configurations sampled at different temperatures, the replica exchange molecular dynamics (REMD) simulation achieves extensive sampling without altering the potential energy surface and without using any collective variables. However, REMD needs a large number of replicas to increase the acceptance probability for configurational swaps, which is computationally taxing, especially for larger molecular systems. By combining equilibrium MD and non-equilibrium work simulations on very few replicas, the replica exchange with non-equilibrium switches (RENS) method increases the acceptance probability and efficiently improves the configurational sampling. The implementation of RENS algorithm with two replicas and its application on the four models systems was explored in this article. The desired equilibrium distributions were reproduced by RENS for all the model systems, and diagrammatically shown for three, whereas REMD and MD simulations could not do so due to inadequate sampling on the same timescales. The work distributions calculated from RENS simulations obeyed the expected non-equilibrium fluctuation theorem of Crooks[46]. The observed f_{sw} vs $< w >$ and f_{sw} vs $< P_{acc} >$ correlations indicate that the switching time of the non-equilibrium simulations can be systematically altered to improve the acceptance probability and the reduced work of switching, while keeping the constraints of the length of the work simulation in mind. The modular implementation of RENS algorithm not only enables us to readily extend it to multiple replicas, but also paves the way for extending it for larger molecular systems in the future.

SUPPLEMENTARY MATERIAL

See supplementary material for the additional KL divergence plots for each particle index, figures containing the overlapping distributions test for each of the individual model systems, and the overlapping distributions test plotted for all 10 RENS simulations of the Lennard-Jones system (Model-IV).

APPENDIX

Appendix A: Propagator for work simulations

If $\mathbf{\Gamma}(t)$ denotes the phase space vector at time t, then the time evolution of the system is governed by the following equation:

$$\mathbf{\Gamma}(\Delta t) = e^{iL\Delta t}\mathbf{\Gamma}(0) \tag{A1}$$

;; where $iL = \dot{\mathbf{q}}.\frac{\partial}{\partial \mathbf{q}} + \dot{\mathbf{p}}.\frac{\partial}{\partial \mathbf{p}}$ is the Liouville operator[32]. If $iL_1 = \dot{\mathbf{q}}.\frac{\partial}{\partial \mathbf{q}}$ and $iL_2 = \dot{\mathbf{p}}.\frac{\partial}{\partial \mathbf{p}}$, then using the Trotter's factorization[33], we obtain the following evolution equation :

$$\mathbf{\Gamma}(\Delta t) = e^{iL_2\Delta t/2}e^{iL_1\Delta t}e^{iL_2\Delta t/2}\mathbf{\Gamma}(0) \tag{A2}$$

For the work simulation, we have

$$\mathbf{p}(\frac{\Delta t}{2}) = e^{iL_2\Delta t/2}\mathbf{p}(0) \tag{A3}$$

$$= e^{\Delta t/2(\mathbf{F}(\mathbf{q}(0))+\dot{\lambda}s_\lambda \mathbf{p}(0)).\frac{\partial}{\partial \mathbf{p}}}\mathbf{p}(0) \tag{A4}$$

here $\mathbf{F}(\mathbf{q}(0))$ is the force evaluated at $t = 0$.

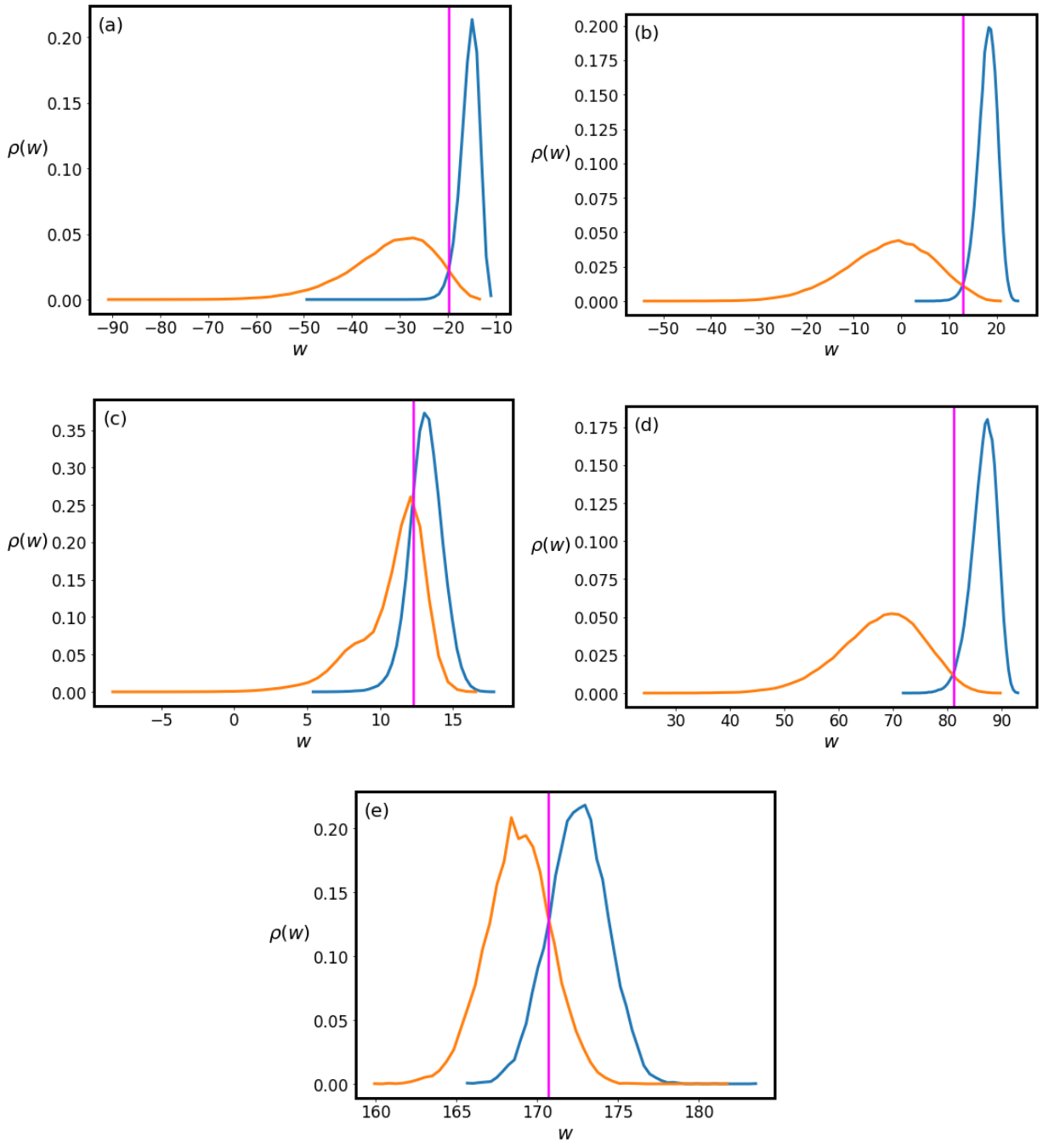

FIG. 11: Work distributions obtained from the heating ($\rho_H(w)$ (blue)) and cooling ($\rho_C(-w)$ (orange)) work simulations of RENS for (a) Model-I (with $\tau = 0.25$), (b) Model-II (with T_A =7, $T_B = 20$, and $\tau = 2.0$), and (c) Model-II (with T_A =7, $T_B =$ 12, and $\tau = 22.0$), (d) Model-III (with $\tau = 0.1$), and (e) Model-IV (with $\tau = 1.5$) The vertical line (magenta) denotes the numerically calculated value of the free energy difference (Δf) between the replicas.

Equation A3 is of the form

$$\mathbf{p}(\frac{\Delta t}{2}) = e^{[t.z.\frac{\partial}{\partial g(\mathbf{p})}]}\mathbf{p}(0) \tag{A5}$$

with

$$g(p) = \ln(a + z.p) \tag{A6}$$
$$t = (\Delta t/2) \tag{A7}$$
$$a = F(q)\,\& \tag{A8}$$
$$z = \dot{\lambda} s_\lambda \tag{A9}$$

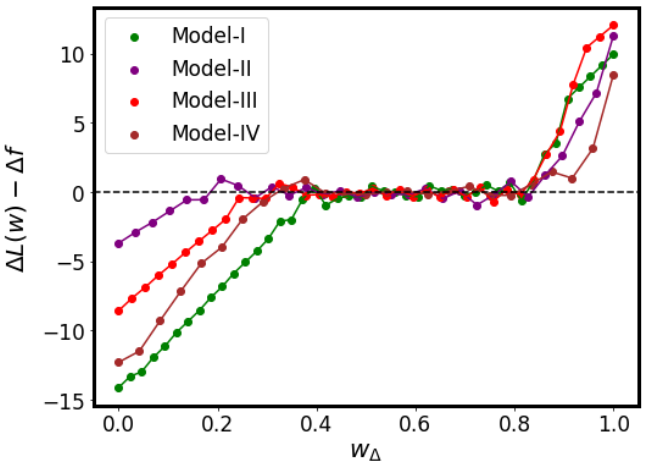

FIG. 12: $\Delta L(w) - \Delta f$ versus w_Δ correlation for all the model systems. The horizontal dashed line corresponds to $\Delta L(w) = \Delta f$.

Equation A5 can be simplified as follows :

$$e^{[t.z.\frac{\partial}{\partial g(p)}]}p \tag{A10}$$
$$= e^{[t.z.\frac{\partial}{\partial g(p)}]}g^{-1}(g(p)) \tag{A11}$$
$$= g^{-1}(g(p) + z.t) \tag{A12}$$

Substituting $g(p)$ into the expression,

$$g^{-1}(g(p) + z.t) = g^{-1}(ln(a + z.p) + b.t) \tag{A13}$$
$$= g^{-1}(\ln\{(a + z.p).e^{z.t}\}) \tag{A14}$$

We have

$$g(p) = \ln(a + b.p) \tag{A15}$$
$$\implies g^{-1}(p) = \frac{e^p - a}{b} \tag{A16}$$
$$\implies g^{-1}(ln(p)) = \frac{p - a}{b} \tag{A17}$$
$$\tag{A18}$$

Hence

$$e^{[t.z.\frac{\partial}{\partial g(p)}]}p = \frac{(a + z.p).e^{z.t} - a}{z} \tag{A19}$$
$$= p.e^{z.t} + a.\frac{(e^{z.t} - 1)}{z} \tag{A20}$$
$$= p.e^{\frac{z.\Delta t}{2}} + F(q).\frac{(e^{\frac{z.\Delta t}{2}} - 1)}{z} \tag{A21}$$
$$\tag{A22}$$

This results in the following update equation :

$$\mathbf{p}(\frac{\Delta t}{2}) = \mathbf{p}(0).e^{\frac{z.\Delta t}{2}} + \mathbf{F}(\mathbf{q}(0)).\frac{(e^{\frac{z.\Delta t}{2}} - 1)}{z} \tag{A23}$$

The update equation for $\mathbf{q}$ follows,

$$e^{iL_1\Delta t}\mathbf{q} = e^{\frac{\mathbf{p}(\frac{\Delta t}{2})}{m}\Delta t\frac{\partial}{\partial \mathbf{q}}}\mathbf{q} \tag{A24}$$
$$= \mathbf{q}(0) + \frac{\mathbf{p}(\frac{\Delta t}{2})}{m}\Delta t \tag{A25}$$

$$\mathbf{q}(\Delta t) = \mathbf{q}(0) + \frac{\mathbf{p}(\frac{\Delta t}{2})}{m}.\Delta t \tag{A26}$$

The last operation of the Liouville operator is the same as the first, which gives us the update equation :

$$\mathbf{p}(\Delta t) = \mathbf{p}(\frac{\Delta t}{2})e^{\frac{z\Delta t}{2}} + \mathbf{F}(\mathbf{q}(\Delta t)).\frac{(e^{\frac{z\Delta t}{2}} - 1)}{z} \tag{A27}$$

Appendix B: Algorithms

Algorithm 2: WorkIntegrator

Input : q_0, p_0, t
Output: $q_{\Delta t}, p_{\Delta t}$
$T_\lambda \leftarrow T_A + \lambda(t).(T_B - T_A)$
$z \leftarrow \dot{\lambda}(t).(1/(2T_\lambda)).(T_B - T_A)$
$p \leftarrow p_t.e^{(z.dt/2)} + (F(q_0)/z).(e^{(z.dt/2)} - 1)$
$q \leftarrow q_0 + (p/m) * dt$
$p \leftarrow p.e^{(z.dt/2)} + (F(q)/z).(e^{(z.dt/2)} - 1)$
return q, p

Algorithm 3: AndersenUpdate

Input : p_t, N, T_λ, m
Output: p_{t+dt}
$ind \leftarrow random(0, N)$
$\beta \leftarrow 1/(kB.T_\lambda)$
$\sigma \leftarrow 1/\sqrt{\beta.m_{ind}}$
$p_{new} \leftarrow p$
$p_{new}[ind] \leftarrow normal(scale = \sigma)$
return p_{new}

Algorithm 1: WorkSimulation

Input : $q, p, N, T_A, T_B, m, \tau, k, dt$
Output: q, p, w
$t \leftarrow 0$
$i \leftarrow 0$
$w \leftarrow -\frac{H(q,p)}{T_A}$
$N_{dof} \leftarrow N.d$
$heat \leftarrow \frac{N_{dof}}{2} \ln \frac{T_B}{T_A}$
do
  $T_\lambda \leftarrow T_A + \lambda(t) * (T_B - T_A)$
  if $i\%k == 0$ **then**
    $p_{new} \leftarrow \text{AndersenUpdate}(p, N, T_\lambda, m)$
    $h_{new} \leftarrow H(q, p_{new})/T_\lambda$
    $h_{old} \leftarrow H(q,p)/T_\lambda$
    $heat \leftarrow heat + (h_{new} - h_{old})$
  end
  else
    $q, p \leftarrow \text{WorkIntegrator}(q, p, t)$
  end
  $t \leftarrow t + dt$
  $i \leftarrow i + 1$
while $t < \tau$;
$w \leftarrow w + H(q,p)/T_B$
$w \leftarrow w - heat$
return q, p, w

TABLE II: Parameters used in the algorithms

Variable	**Explanation**
$\boldsymbol{q}$	Position vector
$\boldsymbol{q_0}$	Position vector at the beginning of the work simulation
$\boldsymbol{q_n}$	Position vector at the end of the work simulation
$\boldsymbol{p}$	Momentum vector
$\boldsymbol{p_0}$	Momentum vector at the beginning of the work simulation
$\boldsymbol{p_n}$	Momentum vector at the end of the work simulation
$\boldsymbol{p_t}$	Momentum vector at time t of the work simulation
$H(\boldsymbol{q}, \boldsymbol{p})$	The Hamiltonian function
$\boldsymbol{m}$	Array of masses
N	Number of particles
T_A	Temperature of the current replica
T_B	Temperature of the conjugate replica
T_λ	The lambda controlled temperature at time t
τ	Switching time for RENS
r	Attempt rate
Δt	Timestep of the simulation
τ	Switching time for RENS
d	System dimension
$traj$	Phase space trajectory of the simulation
$works_f$	Array of reduced works for the forward (heating) work process from T_A to T_B
$works_r$	Array of reduced works for the reverse (cooling) work process from T_B to T_A
$random(0, N)$	A function returning a random integer in the range [0, N)
$normal(scale = \sigma)$	A function which returns a number sampled from the normal distribution with mean 0 and standard deviation σ.

Algorithm 4: RENS

Input : $q, p, m, T_A, N, \tau, r, k, \Delta t, d$
Output: $traj, works_f, works_r$
$mode \leftarrow 0$
$works_f \leftarrow []$
$works_r \leftarrow []$
$t \leftarrow 0$
$nsteps \leftarrow \lfloor \frac{t}{\Delta t} \rfloor$
$i \leftarrow 0$
do
  if $mode == 0$ **then**
    $q, p \leftarrow Thermostat(q, p, m, T, \Delta t)$
    $i \leftarrow i + 1$
    $traj.append(q)$
    $rand \leftarrow random()$
    if $rand <= r * \Delta t$ **then**
      $mode \leftarrow 1$
    end
  else
    $T_B \leftarrow \text{recv}(temperature)$
    $q_n, p_n, w_f \leftarrow$
     $\text{WorkSimulation}(q, p, N, T_A, T_B, m, \tau, k, d)$
    $w_r \leftarrow \text{recv}(w_f)$
    $w \leftarrow w_f + w_r$
    $p \leftarrow min\{1, exp(-w)\}$
    $rand \leftarrow random()$
    if $rand <= p$ **then**
      $q_n, p_n \leftarrow Exchange(q_n, p_n)$
      $q \leftarrow q_n$
      $p \leftarrow p_n$
    end
    $works_f.append(w_f)$
    $works_r.append(w_r)$
    $mode \leftarrow 0$
    $i \leftarrow i + \lfloor \frac{\tau}{\Delta t} \rfloor$
  end
while $i < nsteps$;
return $traj, works_f, works_r$

REFERENCES

[1] M. Iannuzzi, A. Laio, and M. Parrinello, "Efficient exploration of reactive potential energy surfaces using car-parrinello molecular dynamics," Physical Review Letters **90** (2003), 10.1103/physrevlett.90.238302.

[2] A. Tilocca and A. Selloni, "Reaction pathway and free energy barrier for defect-induced water dissociation on the (101) surface of TiO2-anatase," The Journal of Chemical Physics **119**, 7445–7450 (2003).

[3] J. L. Klepeis, K. Lindorff-Larsen, R. O. Dror, and D. E. Shaw, "Long-timescale molecular dynamics simulations of protein structure and function," Current Opinion in Structural Biology **19**, 120–127 (2009).

[4] Y. Duan and P. A. Kollman, "Pathways to a protein folding intermediate observed in a 1-microsecond simulation in aqueous solution," Science **282**, 740–744 (1998).

[5] W. G. Noid, "Perspective: Coarse-grained models for biomolecular systems," The Journal of Chemical Physics **139**, 090901 (2013).

[6] V. Tozzini, "Coarse-grained models for proteins," Current Opinion in Structural Biology **15**, 144–150 (2005).

[7] C. Wu and J.-E. Shea, "Coarse-grained models for protein aggregation," Current Opinion in Structural Biology **21**, 209–220 (2011).

[8] C. Clementi, "Coarse-grained models of protein folding: toy models or predictive tools?" Current Opinion in Structural Biology **18**, 10–15 (2008).

[9] K. Klymko, P. L. Geissler, J. P. Garrahan, and S. Whitelam, "Rare behavior of growth processes via umbrella sampling of trajectories," Physical Review E **97** (2018), 10.1103/physreve.97.032123.

[10] J. Kästner, "Umbrella sampling," Wiley Interdisciplinary Reviews: Computational Molecular Science **1**, 932–942 (2011).

[11] M. Souaille and B. Roux, "Extension to the weighted histogram analysis method: combining umbrella sampling with free energy calculations," Computer Physics Communications **135**, 40–57 (2001).

[12] N. Bhatnagar, G. Kamath, I. Chelst, and J. J. Potoff, "Direct calculation of 1-octanol–water partition coefficients from adaptive biasing force molecular dynamics simulations," The Journal of Chemical Physics **137**, 014502 (2012).

[13] H. Fu, X. Shao, C. Chipot, and W. Cai, "Extended adaptive biasing force algorithm. an on-the-fly implementation for accurate free-energy calculations," Journal of Chemical Theory and Computation **12**, 3506–3513 (2016).

[14] T. Lelièvre, M. Rousset, and G. Stoltz, "Long-time convergence of an adaptive biasing force method," Nonlinearity **21**, 1155–1181 (2008).

[15] A. Barducci, M. Bonomi, and M. Parrinello, "Metadynamics," WIREs Computational Molecular Science **1**, 826–843 (2011).

[16] L. Sutto, S. Marsili, and F. L. Gervasio, "New advances in metadynamics," Wiley Interdisciplinary Reviews: Computational Molecular Science **2**, 771–779 (2012).

[17] M. M. Sultan and V. S. Pande, "tICA-metadynamics: Accelerating metadynamics by using kinetically selected collective variables," Journal of Chemical Theory and Computation **13**, 2440–2447 (2017).

[18] X. Wang, X. Tu, B. Deng, J. Z. H. Zhang, and Z. Sun, "BAR-based optimum adaptive steered MD for configurational sampling," Journal of Computational Chemistry **40**, 1270–1289 (2019).

[19] L. J. Kingsley, J. Esquivel-Rodríguez, Y. Yang, D. Kihara, and M. A. Lill, "Ranking protein–protein docking results using steered molecular dynamics and potential of mean force calculations," Journal of Computational Chemistry **37**, 1861–1865 (2016).

[20] G. Patargias, H. Martay, and W. B. Fischer, "Reconstructing potentials of mean force from short steered molecular dynamics simulations of vpu from HIV-1," Journal of Biomolecular Structure and Dynamics **27**, 1–12 (2009).

[21] Y. Sugita and Y. Okamoto, "Replica-exchange molecular dynamics method for protein folding," Chemical physics letters **314**, 141–151 (1999).

[22] D. A. Kofke, "On the acceptance probability of replica-exchange monte carlo trials," The Journal of Chemical Physics **117**, 6911–6914 (2002).

[23] A. Kone and D. A. Kofke, "Selection of temperature intervals for parallel-tempering simulations," The Journal of Chemical Physics **122**, 206101 (2005).

[24] C. Predescu, M. Predescu, and C. V. Ciobanu, "On the efficiency of exchange in parallel tempering monte carlo simulations," The Journal of Physical Chemistry B **109**, 4189–4196 (2005).

[25] H. Fukunishi, O. Watanabe, and S. Takada, "On the hamiltonian replica exchange method for efficient sampling of biomolecular systems: Application to protein structure prediction," The Journal of Chemical Physics **116**, 9058–9067 (2002).

[26] P. Liu, B. Kim, R. A. Friesner, and B. J. Berne, "Replica exchange with solute tempering: A method for sampling biological systems in explicit water," Proceedings of the National Academy of Sciences **102**, 13749–13754 (2005).

[27] Y. Sugita, A. Kitao, and Y. Okamoto, "Multidimensional replica-exchange method for free-energy calculations," The Journal of Chemical Physics **113**, 6042–6051 (2000).

[28] A. Okur, D. R. Roe, G. Cui, V. Hornak, and C. Simmerling, "Improving convergence of replica-exchange simulations through coupling to a high-temperature structure reservoir," Journal of Chemical Theory and Computation **3**, 557–568 (2007).

[29] S. W. Rick, "Replica exchange with dynamical scaling," The Journal of Chemical Physics **126**, 054102 (2007).

[30] A. J. Ballard and C. Jarzynski, "Replica exchange with nonequilibrium switches," Proceedings of the National Academy of Sciences **106**, 12224–12229 (2009).

[31] E. Weinan and D. Li, "The andersen thermostat in molecular dynamics," Communications on pure and applied mathematics **61**, 96–136 (2008).

[32]G. J. Martyna, M. E. Tuckerman, D. J. Tobias, and M. L. Klein, "Explicit reversible integrators for extended systems dynamics," Molecular Physics **87**, 1117–1157 (1996).
[33]H. F. Trotter, "On the product of semi-groups of operators," Proceedings of the American Mathematical Society **10**, 545–551 (1959).
[34]D. J. Evans and B. L. Holian, "The nose–hoover thermostat," The Journal of Chemical Physics **83**, 4069–4074 (1985).
[35]M. Tuckerman, *Statistical Mechanics: Theory and Molecular Simulation*, Oxford Graduate Texts (OUP Oxford, 2010).
[36]O. Farago, "Langevin thermostat for robust configurational and kinetic sampling," Physica A: Statistical Mechanics and its Applications **534**, 122210 (2019).
[37]B. S. Daan Frenkel, *Understanding molecular simulation: from algorithms to applications* (Elsevier, 2001).
[38]J. P. K. Doye and D. J. Wales, "Saddle points and dynamics of lennard-jones clusters, solids, and supercooled liquids," The Journal of Chemical Physics **116**, 3777–3788 (2002).
[39]D. J. Wales, "Rearrangements of 55-atom lennard-jones and (c60)55 clusters," The Journal of Chemical Physics **101**, 3750–3762 (1994).
[40]K. Ruedenberg and J.-Q. Sun, "Gradient fields of potential energy surfaces," The Journal of Chemical Physics **100**, 5836–5848 (1994).
[41]H. Jónsson, G. Mills, and K. W. Jacobsen, "Nudged elastic band method for finding minimum energy paths of transitions," (385).
[42]A. Rahman, "Correlations in the motion of atoms in liquid argon," Physical review **136**, A405 (1964).
[43]M. Henderson and M. Wertheim, "Phase diagram and pv isotherms of argon," The Journal of Chemical Physics **51**, 5420–5429 (1969).
[44]S. Kullback and R. A. Leibler, "On information and sufficiency," The Annals of Mathematical Statistics **22**, 79–86 (1951).
[45]F. Perez-Cruz, "Kullback-leibler divergence estimation of continuous distributions," in *2008 IEEE International Symposium on Information Theory* (IEEE, 2008).
[46]G. E. Crooks, "Entropy production fluctuation theorem and the nonequilibrium work relation for free energy differences," Physical Review E **60**, 2721–2726 (1999).
[47]A. Pohorille, C. Jarzynski, and C. Chipot, "Good practices in free-energy calculations," The Journal of Physical Chemistry B **114**, 10235–10253 (2010).
[48]A. J. Ballard and C. Jarzynski, "Replica exchange with nonequilibrium switches: Enhancing equilibrium sampling by increasing replica overlap," The Journal of chemical physics **136**, 194101 (2012).